Clays and Clay Minerals, Vol. 57, No. 5, 586–601, 2009.

EFFECT OF THE SIZE OF AGGREGATES ON PORE CHARACTERISTICS OF MINERALS MEASURED BY MERCURY INTRUSION AND WATER-VAPOR DESORPTION TECHNIQUES

GRZEGORZ JOZEFACIUK*

Institute of Agrophysics of the Polish Academy of Sciences, Doswiadczalna 4, 20-290 Lublin, Poland

Abstract—The size, shape, and continuity of pores in mineral solids greatly influence the behavior of percolating liquids and solids in porous media, which has significant practical environmental implications. In order to expand understanding of these properties in soil minerals, the present study was undertaken to analyze the pore characteristics of bentonite, illite, and kaolinite in the forms of powder and aggregates of different dimensions, combining water-vapor desorption and mercury-intrusion techniques. Different granulometric fractions of milled quartz glass were also studied. With increasing aggregate size of the minerals, larger pore volumes (up to 25%), smaller surface areas (down to 15%), larger average radii (up to 15%), and smaller fractal dimensions (down to 6%) were measured using water-vapor adsorption-desorption data. The differences were smallest for bentonite, possibly due to the smallest particle size of this mineral and/or to its very large water-vapor adsorption capacity. The degree of water-vapor adsorption on quartz was too small to rely on the data obtained.

The pore volumes and average radii, measured by mercury-intrusion porosimetry, were up to few times larger for the mineral powders than for their aggregate counterparts. Similar values were noted for aggregates >1 mm in diameter, for which the input of interaggregate spaces into total porosity of the sample bed was negligible. Two pathways of mercury intrusion were detected in porosimetric curves: filling of interaggregate spaces, and penetration into aggregates. Similar penetration thresholds into aggregates of different sizes were calculated. With increasing size of quartz grains, the pore volume of the quartz bed decreased whereas the average pore radius increased. Mercury intrusion detected pore-fractal behavior of bentonite and kaolinite, but for aggregated minerals the calculated values of fractal dimensions were >3, values which increased with increasing aggregate size. Very similar pore parameters were measured for aggregates prepared from a natural deposit of kaolinite and for artificially prepared aggregates from powder of the same mineral, indicating that artificial aggregation can simulate natural processes.

Both water desorption and mercury intrusion detected fractal behavior in the limited range of pores. A test to find fractal build up of the aggregates in extended scales based on a dependence of surface area of unit volume of aggregate bed on aggregate size showed no fractal-aggregate build-up.

Key Words—Aggregate, Adsorption Isotherms, Mercury Intrusion, Mineral, Porosity.

INTRODUCTION

Many natural bodies are highly porous as a result of their complex structure and the granular character of the solid phase. The basic characteristic of such bodies is demonstrated by a pore-size distribution function showing fractions of pores of different radii while the overall amount of pores is characterized by the pore volume or bulk density of the material (Rouquerol *et al.* 1994). The pore system of many porous bodies may be geometrically similar under different magnifications which can be characterized by a fractal dimension (Mandelbrot 1982; Perrier *et al.*, 1999).

The pore properties of solids are determined using so-called 'direct' and 'indirect' methods. Direct methods are based on an analysis of images of cross sections of porous bodies (by reflected or transmitted light microscopy and X-ray diffraction or nuclear magnetic resonance scanning). Indirect methods determine pore systems based on measurements of other physicochemical parameters related to pore sizes and volumes, *e.g.* volume and pressure of gas, vapor, or liquid present within and over the sample of the porous body in equilibrium (Lawrence, 1977; Sing, 1982). Arguably the most frequently used indirect porosimetric methods are mercury intrusion porosimetry (MIP) and vapor desorption isotherms (VD) (Abell *et al.* 1999; Rouquerol *et al.* 1999). Mercury intrusion porosimetry is based on mercury being forced into a sample pore network: by increasing the external pressure, mercury successively invades pore-chamber volumes as an inverse function of their pore-throat radii. The VD is a function relating the amount of adsorbed vapor to its equilibrium pressure during the pressure decrease at a constant temperature. The amount of adsorbate is related to the pore volume and its equilibrium pressure to the pore radius. Frequently, nitrogen and water vapor are used as the adsorbates. While measurement of the isotherm for

* E-mail address of corresponding author:
jozefaci@ipan.lublin.pl
DOI: 10.1346/CCMN.2009.0570507

nitrogen at liquid nitrogen temperature requires advanced instrumental techniques, the water vapor desorption isotherm can be measured at room temperature using a simple vacuum chamber method. Due to the intrinsic features and limitations of the above methods, the MIP detects pores ranging from ~10 μm to 1 nm (for the instrumentation used in the present study, the range was 7.5 μm to 3.75 nm) in size, while the desorption isotherms measured pores from ~1 to a few tens of nm.

Because the size, shape, and continuity of pores affect many important processes in soils, the aforementioned techniques are used increasingly to characterize soil structure and surface properties as well as to quantify modifications to soil structure due to the impact of management practices or degradation processes. Using MIP, Pachepsky *et al.* (1995) characterized the effects of simulated soil degradation (organic matter depletion, cyclic wetting-drying, and silica accumulation) on the pore properties of a soil. Hajnos *et al.* (1999) used MIP to study an effect of organic matter leaching on soil porosity. Jozefaciuk *et al.* (2001b) applied both MIP and VD to observe the effect of various tillage practices on soil-pore parameters. Gomendy *et al.* (1999) used MIP to study structure and its dynamics in tilled, silty topsoil. Using MIP, Cox *et al.* (1997) observed reductions in the porosity of soil aggregates under olive-mill wastewater addition. Mercury intrusion porosimetry was used by Elsharief and Lovel (1996) to estimate the pore-size distribution and porosity of a geotextile filter and by Gorres *et al.* (2001) in a comparative study of the soil structure of a bulk soil and its recycled soil counterpart located in the burrows and casts formed by earthworms. Using MIP, Perez *et al.* (1999) studied structural modification of soil surface by sealing and crusting while Barral *et al.* (1998) studied the effects of Fe and organic matter on porosity and structural stability of aggregates of two cropped soils. Chung and Alexander (1999) studied soil microporosity by VD, finding correlations between the volume of nanopores with organic carbon, clay content, and surface area of the soils. Schaffer *et al.* (1997) used pore-size distribution derived from MIP for modeling gas diffusion in soils. Using both techniques, changes in soil porosity under acid and alkali treatments were studied by Jozefaciuk *et al.* (2002). Changes in pore structure for samples of kaolinite amended with different amounts of humic acid were studied using MIP by Hajnos (1998) and using both MIP and VD by Sokolowska and Sokolowski (1999). Using MIP, Volzone and Hipedinger (1997) studied the effect of high-pressure compaction of kaolinite and montmorillonite samples on their textural characteristics in relation to particle size and cation exchange capacity. Gnanapragasam *et al.* (1995) used VD to study the microstructure of bentonite after the adsorption of aniline. Using both techniques, Hajnos *et al.* (2003) studied a porous system in acidic, sandy, forest soils and Jozefaciuk *et al.* (2001c, 2003) studied the effect of cyclodextrin addition on changes in the pore system of minerals and soils. The VD technique was used by Balci (1999) to study the transformation of sepiolite structure due to the extraction of Fe and Al by acid treatment. Srasra and Trabelsi-Ayedi (2000), Notario *et al.* (1995), Temuujin *et al.* (2004), and Suarez Barrios *et al.* (1995) studied changes in the pore systems of various minerals after acid and alkali treatments.

The pore systems in natural materials are very complex (Ringrose-Voase and Bullock 1984). Pores in granular materials such as soils and/or mineral beds occur around contact points of their particulate components and are constructed from larger chambers accessible through the narrower necks. This is particularly important in MIP measurements because the necks control intrusion of mercury into pore chambers and, therefore, the MIP curves (and the derived pore parameters) may be obscured. In granular media the pore volume accessible through the necks of a hydraulic radius, R, and not the frequency of pores of that size is estimated (Dullien and Dhawan 1975). Hollewand and Gladden (1992) suggested that shielding of large pores by smaller pores leads to an increase in tortuosity and broad pore-size distributions. The intrusion volumes can also be obscured by the sample compression during pressure increase (Lawrence, 1977; Kozak *et al.*,1, 991) and/or by the moisture content of the outgassed samples. The latter, however, can easily be corrected by weighing of the outgassed and completely dried sample (Gomendy *et al.* 1999). In the present studies the samples were dried completely.

Different sample states have been used for mercury intrusion tests of soils and its constituents: powders of minerals (*e.g.* Hajnos, 1998); soils screened by 2 mm sieves (*e.g.* Pachepsky *et al.*, 1995); aggregates of various sizes (*e.g.* Barral *et al.*, 1998; Cox, 1977; Bartoli *et al.*, 1999); and/or undisturbed natural samples (*e.g.* Pagliali *et al.*,1, 995; Perez *et al.*, 1999). Moore and Donaldson (1995) described difficulties in preparing samples of real soils to maintain undisturbed microstructure and evaluating their parameters. To obtain homogeneous soil samples, Fies (1992) placed a wet soil paste on a bed of dry soil aggregates and dried the system for 48 h. That soil-sample dimensions may cause large variation in MIP readings seems rather obvious, and this may be caused by non-uniform composition of aggregates of various sizes, *e.g.* more non-porous quartz grains or more undecomposed plant residues in larger particulates. Even homogeneous aggregates of various sizes may form different beds, which may have serious consequences for description of their textures by MIP. Similar effects of sample aggregation status on the nanopore characteristics measured by VD may also occur, though little published literature describes these problems.

The objective of the present study was, therefore, to test the effect of the size of the selected minerals aggregates on MIP and VD pore characteristics of

mineral aggregate beds. The most common soil minerals were selected for these studies: bentonite, illite, and kaolinite.

MATERIALS

Minerals

Bentonite (B, Zebiec, Poland) containing >95% smectite, kaolinite (K, Vimianzo, Spain) containing >90% kaolinite and ~5% quartz, and illite (I, Yongdong, Korea) comprising ~70% mica and ~20% kaolinite-chlorite were studied. The minerals in powder form were water saturated and the cakes obtained were formed into large rolls (~10 mm × 50 mm) by hand. These rolls were wetted and dried four times to stabilize the structure, crushed gently with a knife to minimize artifacts produced due to material compaction during grinding, and screened using a set of sieves: 4, 2, 1, 0.5, 0.25, and 0.09 mm (VEB Metallweberei, Neustadt/Orla, Germany) and the resulting aggregates were collected. The names of the aggregates of dimensions between 4 and 2 mm were abbreviated with the number 1 (*e.g.* B1 for bentonite), aggregates between 2 and 1 mm are abbreviated with number 2, *etc*., up to 6 for aggregates of <0.09 mm. Minerals in powder forms were abbreviated with the letter p (*e.g.* Bp is bentonite powder). Aggregates prepared from natural deposits of the same kaolinite (KN) were also studied.

Quartz

A laboratory quartz glass (Q) was milled on a rotary mill and subdivided, by sieving, into 0.2–0.1, 0.02–0.01, and <0.002 mm (sedimentation) fractions. As the fractions were in different size ranges than the mineral aggregates studied, they are referred to below as Q_{sand}, Q_{silt}, and Q_{clay}, respectively, as is the case in soil-science nomenclature. Quartz was used as a reference, non-porous material having pores only between grains.

Hereafter, the diameter of particular aggregates and of silt and sand quartz grains was taken as the arithmetical average of their maximum and minimum dimensions. The average diameter of the studied powders (bentonite 13.21; illite 18.54; kaolinite 13.23, and clay quartz 5.36 μm) was calculated from laser particle-size analysis data obtained using a Malvern 2000 instrument.

METHODS

Water-vapor adsorption-desorption isotherms and their analysis

Water-vapor adsorption and desorption isotherms were measured in triplicate using the vacuum chamber method (Sokolowska and Sokolowski, 1999) at temperature $T = 294 \pm 0.1$ K. Sample aliquots were transferred to weighing vessels which were placed in a vacuum chamber outgassed to ~100 Pa. The relative water-vapor pressure, p/p_o (p is the equilibrium vapor pressure over the sample and p_o is the saturated vapor pressure at the temperature of the measurements) in the chamber was controlled by sulfuric acid solutions, increased stepwise in terms of concentration (*i.e.* decreasing p/p_o). The amount of water present in the samples, a(kg/kg), at a given p/p_o (calculated from the equilibrium density of H_2SO_4) was measured by weighing after 48 h of equilibration. The adsorption data were taken after completing the desorption measurements using decreasing concentrations of sulfuric acid. The dry mass of the samples was estimated after completing adsorption measurements, after 24 h of oven drying at 378 K. The differences between triplicate measurements of the isotherms did not exceed 1%. The pores detected by VD are referred to hereafter as nanopores.

The equivalent nanopore radius r_N, calculated from desorption isotherms, was related to the desorption pressure p by the Kelvin equation for the hemispherical meniscus:

$$r_N = 2M\,\sigma_W \cos\alpha_W/\rho R T \ln(p_o/p) \quad (1)$$

where M is molecular mass of water, σ_W is water surface tension, α_W is a water-solid contact angle (assumed here to be zero), ρ is density of water, R is the universal gas constant, and T is the temperature of the measurements. The minimum nanopore radius was taken as 1 nm corresponding to $p/p_o = 0.342$. This meets a frequently made assumption that at p/p_o <~0.35 surface adsorption processes dominate and the condensation of vapors in pores occurs at higher relative pressures. The maximum nanopore radius was taken as 50 nm corresponding to $p/p_o = 0.979$. Above this value the differences in the density of the sulfuric acid were small so p/p_o values could not be estimated precisely. Estimation of pore size from water-vapor adsorption data may be obscured by mineral swelling, which may occur in the bentonite studied. Swelling starts, however, when the thickness of water exceeds ~1 nm distance from the basal plane surface (Sposito, 1984), *i.e.* six water layers. For the bentonite studied, such an amount of water may be adsorbed at relative water-vapor pressures >0.96, *i.e.* at the end of the experimental window. Swelling occurs, in particular, if monovalent surface cations are present. The bentonite studied contains a small amount of free carbonates so Ca was expected to be the dominant exchange cation, which retards swelling.

The volume of the pores at a given radius, $v(r)$, was taken as the amount of water accumulated in the material at a given (radius-corresponding) pressure, which was treated as the sum of pore volumes, $v_i(r_i)$, of the radii $r_i \leqslant r$:

$$v(r) = \sum_{i=1}^{n} v_i(r_i). \quad (2)$$

Dividing the above equation by the total pore volume, v_t, the scaled pore volume *vs*. radius curve, $\xi(r)$, was treated as a sum of fractions of particular pores, $f(r_i)$,

which was normalized to 1 throughout the whole experimental window:

$$\Xi(r) = v(r)/v_t = \sum_{i=1}^{n} v_i(r_i)/v_t = \sum_{i=1}^{n} f(r_i) = 1 \quad (3)$$

Thus the pore fraction in a given range of pore sizes was calculated as:

$$f(r_{i,av}) = [\Xi(r_{i+1}) - \Xi(r_i)] \quad (4)$$

where $r_{i,av}$ denotes the arithmetic mean of r_{i+1} and r_i. Knowing the latter values, a pore-size distribution function, *i.e.* pore fraction *vs*. pore-radius dependence, was constructed. These functions were constructed by calculating the amounts (fractions) of pores in five ranges of pore radii (equal in logarithmic scale) which provided similar pore-size distribution functions for the replicates of data.

The average pore radius, r_{av}, was calculated as:

$$r_{av} = \sum_{i=1}^{n} r_i f(r_i) \quad (5)$$

The nanopore fractal dimensions, D_N, were estimated using the Frenkel-Hill-Halsey (FHH) scaling law applied to adsorption of water vapor at each aggegate size. This is a sound approach because, as stated by Rouquerol *et al.* (1999, p. 185), "Pfeifer and his co-workers point out that the interpretation of a fractal dimension of a porous surface presents problems when it is associated with the BET theory. In contrast, an FHH-fractal treatment appears more promising, provided that wetting effects are taken into account." The D_N values were calculated from the slopes of the linear parts (if any) of the ln-ln plots of adsorption *a vs*. adsorption potential $A = RT\ln(p_o/p)$, using the equation:

$$\ln(a) = B - (1/m)\ln(A) \quad (6)$$

where B is a constant and the parameter m is related to the surface fractal dimension of the sample. The magnitude of the parameter $1/m$ distinguishes two possible adsorption regimes (Jaroniec *et al.*, 1997; Jarzebski *et al.*, 1997): when $1/m < 1/3$, the adsorption occurs within the van der Waals regime and the surface fractal dimension is then $D_N = 3(1 - 1/m)$. Alternatively, for $1/m > 1/3$, the adsorption is governed by the capillary condensation mechanism and $D_N = 3 - 1/m$.

Equation 6 should be applied to the experimental data measured within a multilayer adsorption region, *i.e.* for relatively large relative pressures (Neimark, 1996). Within this region the effects of energetic surface heterogeneity play a negligible role, because the surface molecule interactions are screened by the already adsorbed particles.

The monolayer capacities, a_m, of the minerals studied were determined from desorption data using the linear form of the BET equation:

$$p/p_o[a(1 - p/p_o)]^{-1} = (Ca_m)^{-1} + p/p_o\,(C - 1)(Ca_m)^{-1} \quad (7)$$

where C is a constant related to adsorption anergy. From a_m values, the surface areas, S, were calculated:

$$S = 3612a_m \quad (8)$$

where the coefficient 3612 is calculated assuming the cross-sectional area of a single water molecule is 10.8×10^{-20} m^2.

Knowing the surface areas of the minerals studied, an alternative method of estimating their fractal properties can be applied (Avnir *et al.*, 1985; Van Damme *et al.*, 1986) based on a concept that if a fractal body is fractioned into granules of different sizes, the surface area of the same volume $S_{/V/}$ of the bed formed from particular fractions increases with a decrease in the granule radius, R, obeying a power law with exponent proportional to the solid surface fractal dimension, D_{ss}. Following van Damme (1998), who generalized for mineral aggregates the analysis that was extensively applied by Avnir *et al.* (1985), the following possible scaling law was derived and validated:

$$S_{/V/} \sim R^{(D_{ss} - D_m)} \quad (9)$$

where $S_{/V/} = S^*\rho_d$ (ρ_d is the bulk density of the aggregate bed, and D_m is the mass fractal dimension). Van Damme and co-workers found that $D_m = 3$ for the selected kaolinite, sepiolite, and palygorskite samples (rigid clay minerals, as are the kaolinite and illite in the present study) and the 20 mono-ionic montmorillontes (similar to the bentonite studied) demonstrating that the mass distribution and the total (open + closed) pore volume (its complement) distribution within the grains are homogeneous. These clay mineral samples were, therefore, neither mass nor total pore volume fractals, in which case equation 9 can be simplified to:

$$S_{/V/} \sim R^{(D_s - 3)} \quad (10)$$

The D_s value can thus be calculated from the slope of equation 10 if plotted in logarithmic coordinates. To calculate D_{ss}, the bulk density was estimated by measuring the volume occupied by a given mass of the aggregates (powder) poured into a measuring glass tube. The bed was not shaken in order to avoid destruction of illite aggregates of extremely low mechanical resistance.

Mercury intrusion curves and their analysis

Mercury intrusion tests were performed for pressures ranging from 0.1 to 200 MPa using a Carlo Erba 2000 pore-size mercury intrusion porosimeter, equivalent to pore radii of $3.75 - 7.5 \times 10^3$ nm. The differences between triplicate measurements of the porosimetric curves did not exceed 3.6% and these were greater for smaller aggregates. The pores detected by MIP are referred to hereafter as mesopores.

Using MIP, the equivalent mesopore radius r_M was related to the mercury intrusion pressure P by the Washburn equation:

$$r_M = -2\sigma_M \cos\alpha_M/P \quad (11)$$

where σ_M is mercury surface tension and α_M is the mercury-solid contact angle.

In general, incorporation of the measured contact angle is essential for a proper textural characterization of porous solids by MIP. In the present studies the common contact angle value of 141.3º was assumed for all samples, which may have led to some uncertainty in pore radii estimation; all relations of pore parameters due to aggregate sizes are valid. Such an assumption was confirmed by the work of Groena *et al.* (2002) who demonstrated that the contact angle of mercury on most oxidic materials, including Al_2O_3 and SiO_2, presented a contact angle close to 140º. Only the contact angle of different carbon samples ($\geqslant$150º) and cement-like materials ($\leqslant$130º) differed significantly from this value.

The mesopore size-distribution functions and average mesopore radii were calculated in the same way as for water-vapor desorption data (equations 2−5), though, due to the greater precision of the measurements, the calculations of pore-size distribution functions (equation 4) were based on subranges equal to 0.2 in logarithmic scale.

The penetration thresholds for the pores inside the aggregates (*i.e.* the points at which mercury starts to enter the aggregates) were approximated by the pore radii at which the second derivative of pore volume *vs*. log radius equals zero:

$$d^2V/d(\log r)^2 = 0 \qquad (12)$$

The mesopore surface fractal dimensions D_M were calculated from mercury intrusion data, from the slopes of the linear parts (if any) of log-log plots of the first derivative of pore volume dependence on radius *vs*. radius using the following dependence :

$$D_M = 2 - d\log[dv(r)/dr)]/d\log r \qquad (13)$$

Where needed in any of the above calculations to define linearity ranges, the procedure of Yokoya *et al.* (1989) was applied. According to this procedure, the measure of linearity, L, for the set of the points in a plane is:

$$L = (4\sigma_{xy}^2 + (\sigma_{yy} - \sigma_{xx})^2)^{1/2} (\sigma_{yy} + \sigma_{xx})^{-1} \qquad (14)$$

where σ_{xx}, σ_{yy}, and σ_{xy} are the variances of x-coordinates and y-coordinates and the covariance between x and y coordinate sets, respectively. The L value falls between 0 (for uncorrelated and random points) and 1 (for points on a straight line). To separate linearity ranges, the value of L is computed for the first three points, then for the first four, five, and so on until the value of L increases. The end of the linearity range is in the points after which the value of L begins to decrease. Similarly, the next linearity range (if any) may be detected for other points not included in the first range. From any given linearity range, the two first and/or last two points were rejected if this caused an increase in the linear regression coefficient for the data set being considered.

The pore volume *vs*. radius curves measured by mercury intrusion and water-vapor desorption usually do not coincide. The measured pore volumes in the common range of pore sizes are quite different and sometimes MIP volumes are greater than those of VD, and sometimes less (Józefaciuk, 2001a). The two methods, therefore, are discussed separately below.

RESULTS AND DISCUSSION

Analysis of water-vapor adsorption-desorption data

Focus, in the present study, was placed on the water-vapor desorption isotherms because only small hysteresis loops were observed from the recorded water-vapor adsorption-desorption isotherms (*e.g.* Figure 1). All water-vapor desorption isotherms were characterized

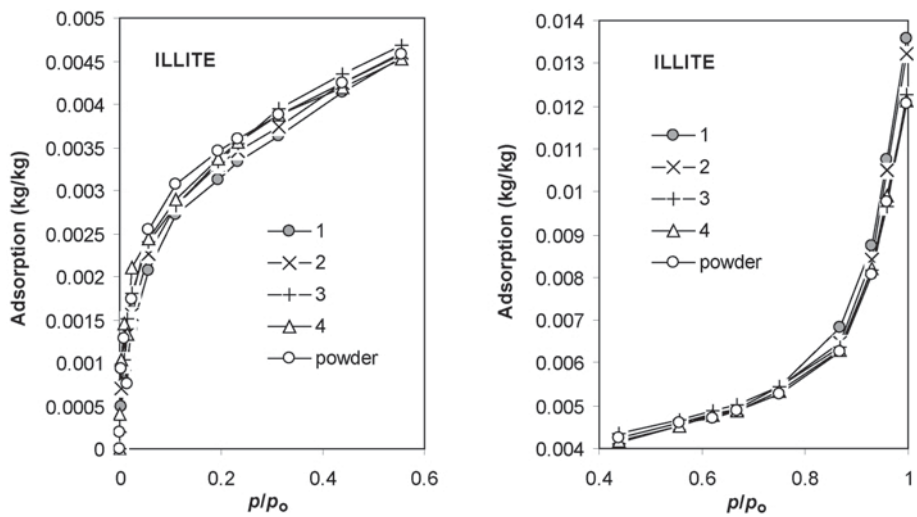

Figure 1. Water-vapor desorption (VD) sigmoidal isotherms for illite powder and aggregates (1 = 2−4 mm, 2 = 1−2 mm, 3 = 0.5−1 mm, and 4 = 0.25−0.5 mm).

by sigmoidal curves (second type in the BET classification of adsorption-desorption isotherms). The adsorption of water vapor on quartz was negligible due to the extremely small porosity and surface area of the material. The amount of water present in the samples, particularly at greater relative pressures, appeared to increase with increasing aggregate sizes, probably due to the input of condensed water in the pores formed between mineral particles within aggregates. At small relative pressures, the opposite tendency was observed (Figure 1). Micropore parameters and surface areas calculated from the isotherms for powder forms of the minerals studied are reported in Table 1. The BET surface areas decreased from bentonite (74 m^2g^{-1}), to kaolinite (23 m^2g^{-1}), and then to illite (10 m^2g^{-1}). Concomitantly, both nanopore volume and surface fractal dimension increased as a function of specific surface area.

Aggregation of the minerals leads to decreases in surface area as revealed in Figure 2. For the largest aggregates of kaolinite, this decrease is ~10% of the surface area of the powdered mineral and for illite and bentonite a somewhat smaller decrease was observed. Such decreases in surface area can probably be attributed to closing of the smallest pores within aggregates by mineral particles. A retardation of water-vapor diffusion into the aggregate body is also possible, however. That surface areas do not depend significantly on the aggregate size may indicate their similar internal build-up on the level below a few nanometers (where the BET equation works). Mineral aggregation leads to an increase in the micropore volume (Figure 3). This increase is greatest for illite: for the largest aggregates it reaches ~25% of the micropore volume of the powdered mineral; smaller for kaolinite, ~20%; and smallest for bentonite, ~12%.

Aggregation of minerals and increase in water condensation at greater relative pressures also cause an increase in the calculated values of average micropore radius (Figure 4). The relative differences in pore radii are twice as small as those in micropore volumes. It seems that an increase in micropore radius should work in parallel with micropore volume increase but these are greatest for kaolinite and not for illite. The observed discrepancy may be due to varying pore-size distributions within mineral aggregates. Nanopore fractal dimensions of the studied minerals (equation 6) decrease with increase in aggregate size (Figure 5). A significant decrease for illite to a D_N value of ~2.07 and a moderate decrease for both kaolinite and bentonite to 2.45 and 2.53, respectively, indicate smoother nanopore surfaces and more compact porous media, explaining the observed decrease in specific (accessible) surface area as a function of aggregate size (Figure 2). Indeed, the surface area appears to decrease linearly with the nanopore fractal dimension decrease (Figure 6). The less rugose the nanopore surface, the less accessible is the surface area.

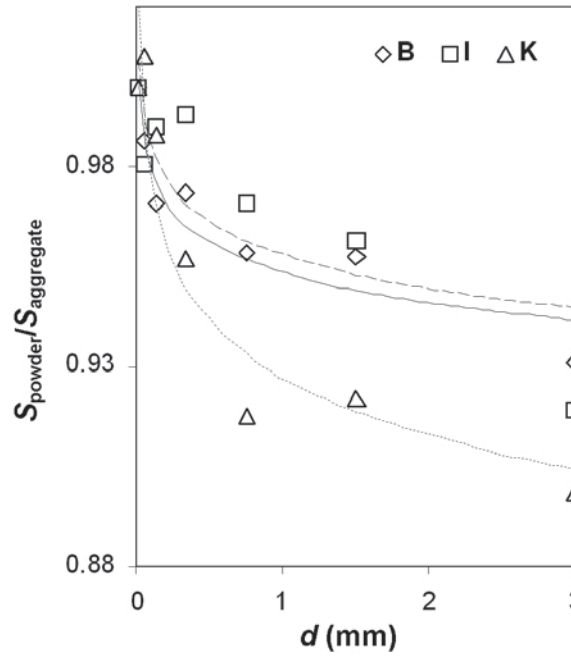

Figure 2. Normalized specific surface area (S aggregate to S powder ratio) as a function of the mineral aggregate size, d. I = illite, K = kaolinite and B = bentonite. The S values of the I, K, and B powders are listed in Table 1. The fitting power law curves are as follows: long dashes – illite, solid line – bentonite, and short dashes – kaolinite.

An attempt to find pore-surface fractal dimensions of the minerals from equation 10 failed. From the log-log dependence of surface area S_{Vl} on aggregate size, the

Table 1. Surface areas and micropore parameters (1–50 nm range) for powders of the minerals studied calculated from water-vapor desorption isotherms.

	Bentonite	Kaolin	Illite
BET surface area (m^2 g^{-1})	74	23	10
Nanopore volume (dm^3 kg^{-1})	0.124	0.055	0.007
Nanopore radius (nm)	8.5	16.7	14.5
Nanopore fractal dimension	2.57*	2.49*	2.21**

*capillary condensation regime, ** van der Waals regime

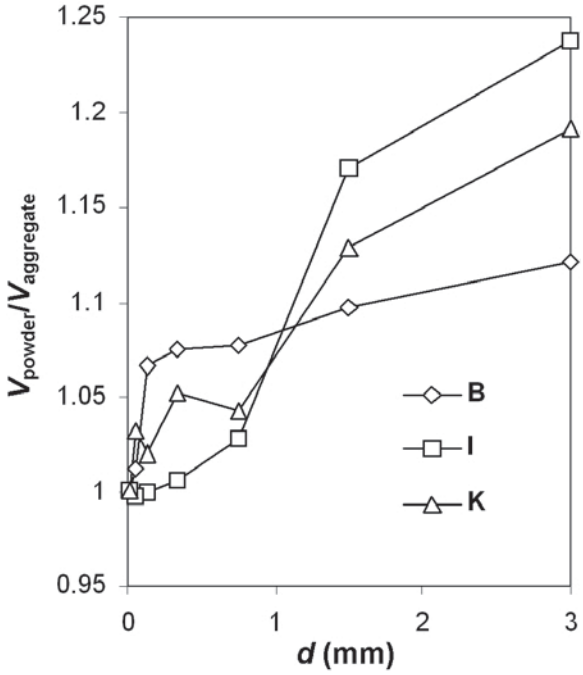

Figure 3. Normalized nanopore (1−50 nm pore radii) volume (V_N aggregate to V_N powder ratio) as a function of the mineral aggregate size, d. I = illite, K = kaolinite and B = bentonite. The V_N values of the I, K, and B powders are listed in Table 1.

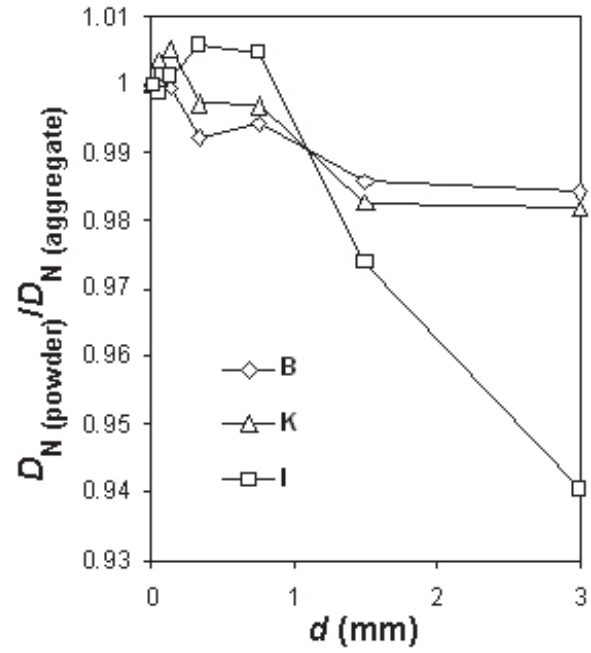

Figure 5. Normalized nanopore surface fractal dimension (D_N aggregate to D_N powder ratio) as a function of the mineral aggregate size, d. I = illite, K = kaolinite, and B = bentonite. R = hydraulic radius. The D_N values of the I, K, and B powders are listed in Table 1.

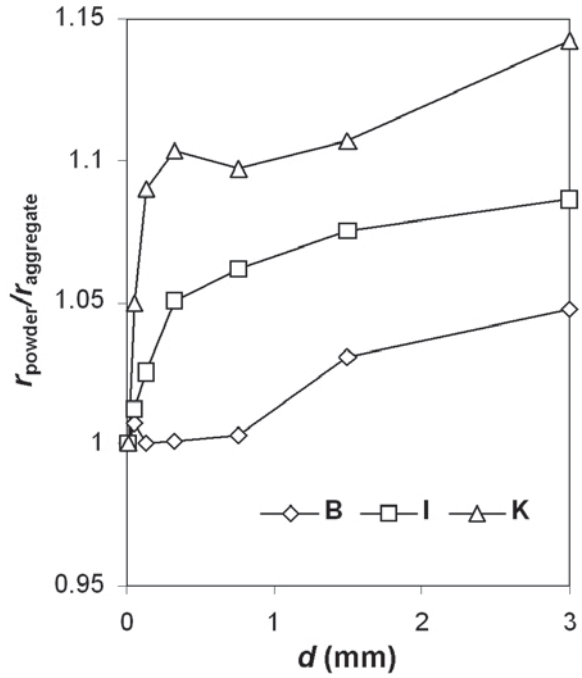

Figure 4. Normalized nanopore radius (r_N aggregate to r_N powder ratio) as a function of the mineral aggregate size, d. I = illite, K = kaolinite, and B = bentonite. The r_N values of the I, K, and B powders are listed in Table 1.

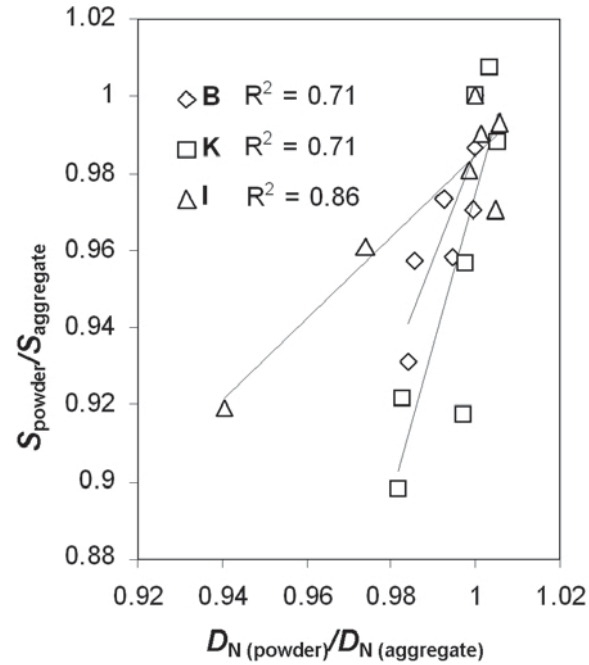

Figure 6. Relation between normalized specific surface area (S aggregate to S powder ratio) and normalized nanopore surface fractal dimension (D_N aggregate to D_N powder ratio) together with straight-linear data fits.

D_{ss} values >3 were estimated. Large D_{ss} values are a direct consequence of small changes in surface areas and simultaneous decrease in bulk density of the aggregate beds with decrease in aggregate size. The bulk density, ρ_d, of the beds decreases for bentonite from 0.87g cm^{-3} (4−2mm aggregates) to 0.80 g cm^{-3} (powder), for illite from 0.77 g cm^{-3} to 0.53 g cm^{-3}, and for kaolinite from 0.71 g cm^{-3} to 0.43 g cm^{-3}, implying that the porosity of the mineral bed (as equal to 1 minus bulk density/solid density) increases with aggregate-size decrease. A slight increase in aggregate bed density (as should be expected in the case of fractal bodies) was observed only for 1−0.5 mm aggregates (0.89 g cm^{-3} for bentonite, 0.79 for illite, and 0.73 for kaolinite). That the bulk density decreases more quickly than the surface area increases means that the $S_{V/}$ decreases with decreasing aggregate size (Figure 2) and, for a fractioned fractal body, this should increase. Pore fractal behavior does not extend to the whole aggregate structure but is limited to a narrow pore range. The measured bulk densities, particularly for illite and kaolinite, are very small, corresponding to extremely porous systems (the porosities of the beds are ~0.7−0.8 cm^3 cm^{-3}). The porosity comprises interaggregate and intra-aggregate porosity. As shown by the mercury-intrusion results (described below) the inter-aggregate porosity of the above minerals is at least 0.4 cm^3 cm^{-3}, so the intra-aggregate porosity should reach a similar magnitude. Such small densities can also be found under natural conditions. Baumann and Keller (1975) reported bulk densities of aggregates of sedimentary kaolin accumulations of 0.8−1.8 cm^3 cm^{-3}.

Analysis of mercury intrusion data

The mercury intrusion curves depended heavily on the aggregate size of the minerals and on the particle size of the quartz (Figure 7) − the smaller the size of the aggregate or quartz particle, the larger the amount of

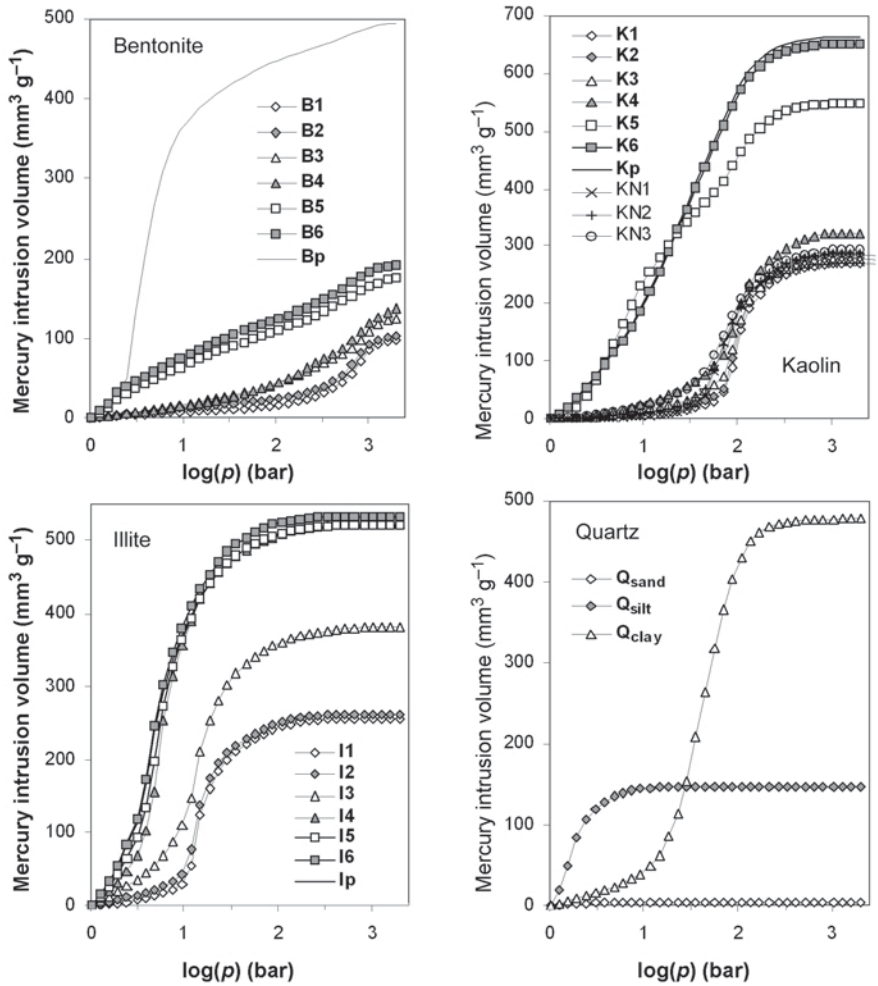

Figure 7. Mercury intrusion porosimetry (MIP) curves for the minerals and quartz studied. The number written next to the mineral abbreviation denotes the size of the aggregate: 1: 4−2 mm; 2: 2−1 mm; 3: 1−0.5 mm; 4: 0.5−0.25 mm; 5: 0.25−0.09 mm; 6: <0.09. The letter p indicates powder. I = illite, K = kaolinite, KN-natural deposit of K, B = bentonite, and Q = quartz.

mercury intruded into the unit mass of the sample at a given pressure. Very similar mercury intrusion curves were measured for the largest (4−2 and 2−1 mm) aggregates of particular minerals. The mercury intrusion curves for the aggregates of the natural deposit of kaolinite are very similar to those of the artificially prepared aggregates, possibly indicating that the method of preparation of the aggregate simulates the natural means of mineral-deposit formation. The properties of the mineral aggregates may depend on method of preparation. Gluba *et al.* (2004) and Heim *et al.* (2005) reported that the bulk density of mineral aggregates varied as a function of either initial moisture and/or wetting time during drum granulation.

In general, the mercury intrusion curves have similar character for all of the materials studied. Initially, a monotonic increase in the volume of the mercury intruded was observed, followed by a rapid increase then the mercury volume tended to reach a plateau − the smaller the mineral aggregate size, the less the pressure at which mercury starts to enter into the pore network of the sample bed and the faster the initial increase in the volume of intruded mercury. This may be related to the fact that mercury first penetrates into the pores located between aggregates and then into the intra-aggregate pores of radii <7.5 μm. Some evidence of the occurrence of both processes was apparent in mercury intrusion curves for the B5 and B6 aggregates for which, after an initial monotonic increase, a rapid increase in the volume of intruded mercury appeared at a similar pressure (pore radius) as for larger aggregates. A similar phenomenon was observed for K5. Clearly, two main types of pore filling exist: (1) the main intrusion of mercury into the interconnected pore networks of the clayey aggregates (B1 to B4, K1 to K4, I1 to I3) (as read from particle-size distributions, some of the Q_{clay} bed may also act in a similar way to a clayey aggregate; see Figure 9); and (2) artifacts related to the invasion of mercury into relatively large pores between the aggregates (main process for the finest aggregates and grains). Looking at the type 1 pore filling (for the largest clayey aggregates), and following Thompson *et al.* (1987), the initial part of the mercury injection curve was associated with "surface defects" (before breakthrough, the invasion was limited to the pores located at the aggregates' surfaces). By contrast, the collection of the smallest clayey aggregates were characteristic of inter-aggregate porosity (Bartoli *et al.*, 1999).

If one assumes that the intrinsic structure of the aggregate does not depend on the aggregate size (this seems rational because individual mineral particles should be much smaller than the aggregates and all aggregates come from crushing of the same mineral bed), the penetration into the aggregates of that same mineral should occur at the same pore radius. Because the quick increase in the porosimetric curves occurs at similar pressures for all large aggregates (Figure 7), it is assumed to correspond with intra-aggregate penetration, so the inflection point on the mercury intrusion curve (condition formulated in equation 12) approximates the aggregate-penetration threshold (Thompson *et al.*, 1987). Very similar values of penetration thresholds for bentonite (B1 to B6, ~15 nm), kaolinite (K1 to K5, ~110 nm), and illite (I1 to I3 ~900 nm) aggregates were observed (Table 2). The pore sizes delimiting the region for intra-aggregate zones apparently depend on the kind of mineral and its individual grain sizes. Romero *et al.* (1999), studying mercury intrusion and extrusion pathways for natural kaolinite-illite-smectite clay, suggested that pore sizes of 130−180 nm can be accepted as the delimiting region separating inter- and intra-aggregate zones, and this information was used to define the 'intra-aggregate governing suction' zone of the water retention curve. The present results correspond to the Romero 'range'. On the curve of K5, two inflection points occurred. The point for larger radii probably corresponds to penetration of the sample bed. The existence of the inflection point for mineral powders at large pore radii (small pressures) may also be due to penetration of the powder bed.

The MIP curves for loose beds formed from quartz grains probably reflect a penetration of zones between individual grains; the grains themselves have no internal porosity. The mercury intrusion curves of non-porous quartz grains could be used as a reference to be subtracted from the curves of mineral aggregates, thus giving intra-aggregate penetration curves. This idea failed, however, because negative pore volume values were calculated for mineral aggregates of similar sizes to those of the quartz grains.

Total mesopore volumes of the samples studied, read from mercury intrusion curves, decreased with increase in aggregate/particle size (Figure 8). Large aggregates of bentonite have the smallest porosity among the minerals studied. A value of ~100 $mm^3\ g^{-1}$ for the aggregates gives (assuming that no pores between aggregates are measured) ~21.0% of the bulk aggregate volume (v/v). Large aggregates of kaolinite and illite have similar porosity, ~40% v/v. The small porosity of the bentonite aggregate may be due to the broad size distribution of mineral particles (smaller particles occupy pores between larger particles, thus the internal porosity of the aggregates decreases) or to their very non-spherical shape. The wetting-drying cycles may have caused specific orientation of the bentonite grains in contact with each other on flat plains, thereby reducing the total pore volume also.

Extremely large (>480 $mm^3 g^{-1}$) pore volumes for beds of the powder forms of minerals and clay-size quartz, which gave >56% v/v porosity, may indicate that many such particles are not in close contact with their neighbors, thus forming large cavities within powder beds. It is also possible that additional pores are formed between the wall of the measuring chamber and

Table 2. Pore radii at penetration threshold (*PT*), pore ranges of fractal behavior (*FR*) and radii of dominant pores (R_d) measured from mercury intrusion curves. The *PT* values (bold) correspond to penetration into aggregates.

Bentonite	B1	B2	B3	B4	B5	B6	Bp
PT (μm)	**0.013**	**0.014**	**0.013**	**0.013**	**0.020**	**0.018**	4
FR (μm)	0.5–0.013	0.8–0.016	10–0.013	10–0.013	4.0–0.013	4.0–1.26	0.8–0.01
R_d (μm)	0.009	0.011	0.011	0.009	5.6	5.6	3.5

Kaolinite	K1	K2	K3	K4	K5	K6	Kp	KN1	KN2	KN3
PT (μm)	**0.11**	**0.11**	**0.11**	**0.11**	**0.11**2.2	0.40	0.40	**0.18**	**0.18**	**0.18**
FR (μm)	10–0.25	7.5–0.20	3.2–0.20	3.2–0.16	6.3–0.13	4.0–0.20	4.0–0.20	2.5–0.20	2.5–0.20	2.0–0.20
R_d (μm)	0.089	0.089	0.089	0.089	1.8	0.56	0.22	0.14	0.14	0.14

Illite	I1	I2	I3	I4	I5	I6	Ip
PT (μm)	**0.89**	**0.89**	**0.89**	2.2	2.3	2.8	2.8
R_d (μm)	0.71	0.71	0.71	1.8	1.8	2.2	2.2
FR (μm)	0.9–0.06	0.6 to 0.06	0.9–0.02	2.2 to 0.06	2.3–0.04	2.8–0.04	2.8–0.04
D_M	1.94	2.02	2.01	2.04	2.03	2.02	2.03

Quartz	Q_{sand}	Q_{silt}	Q_{clay}
PT (μm)	7.1	5.0	2.8
R_d (μm)	5.6	5.6	0.22
FR (μm)	6.3–1.25	5.0–1.25	0.16 to 0.025
D_M	1.95	1.93	1.93

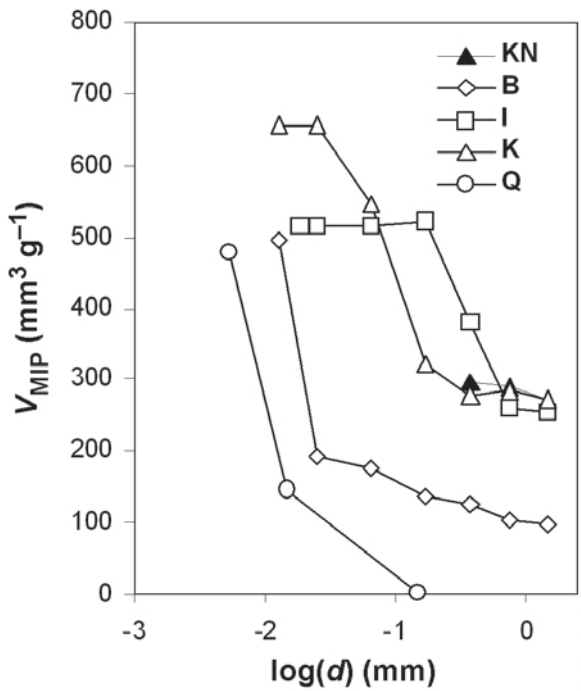

Figure 8. Mesopore (0.03–10 μm) volumes calculated from MIP for the minerals studied and quartz as related to aggregate (particle) size. I = illite, K = kaolinite, KN-natural deposit of K, B = bentonite, and Q = quartz.

individual mineral (quartz) particles 'smeared' over the chamber wall during filling with mercury.

The normalized mesopore-size distribution (PSD) functions (Figure 9) revealed that the largest pores occurred within illite aggregates (the PSD peak is developed at ~0.71 μm), medium in kaolinite (~0.09 μm), and smallest in bentonite (~0.01 μm). The size of these pores may reflect the size of the individual mineral particles – the larger the pore, the larger the particle. Also, the smaller the aggregates, the broader the peaks in the PSD functions observed, probably reflecting the influence of pores in inter-aggregate volumes. However, aggregate crushing during pressure intrusion may lead to a similar peak-broadening effect (Penumadu and Dean, 2000). As the size of the aggregates increases, the resistance towards crushing may increase as was observed by Alie *et al.* (2001) for aggregated low-density silica xerogel particles. Illite aggregates of <0.25 mm and kaolinite aggregates of <0.09 mm have similar PSD functions to the powders of the respective minerals, which probably indicates mechanical destruction of the aggregates to powders during sieving (in Figure 7, for kaolinite, the PSD curve for powder is very close to K6 and for illite it coincides with I6). In the PSD functions of bentonite, a peak at small pore size range developed even for the smallest aggregates (<0.09 mm), indicating that some of the aggregate structure survived sieving.

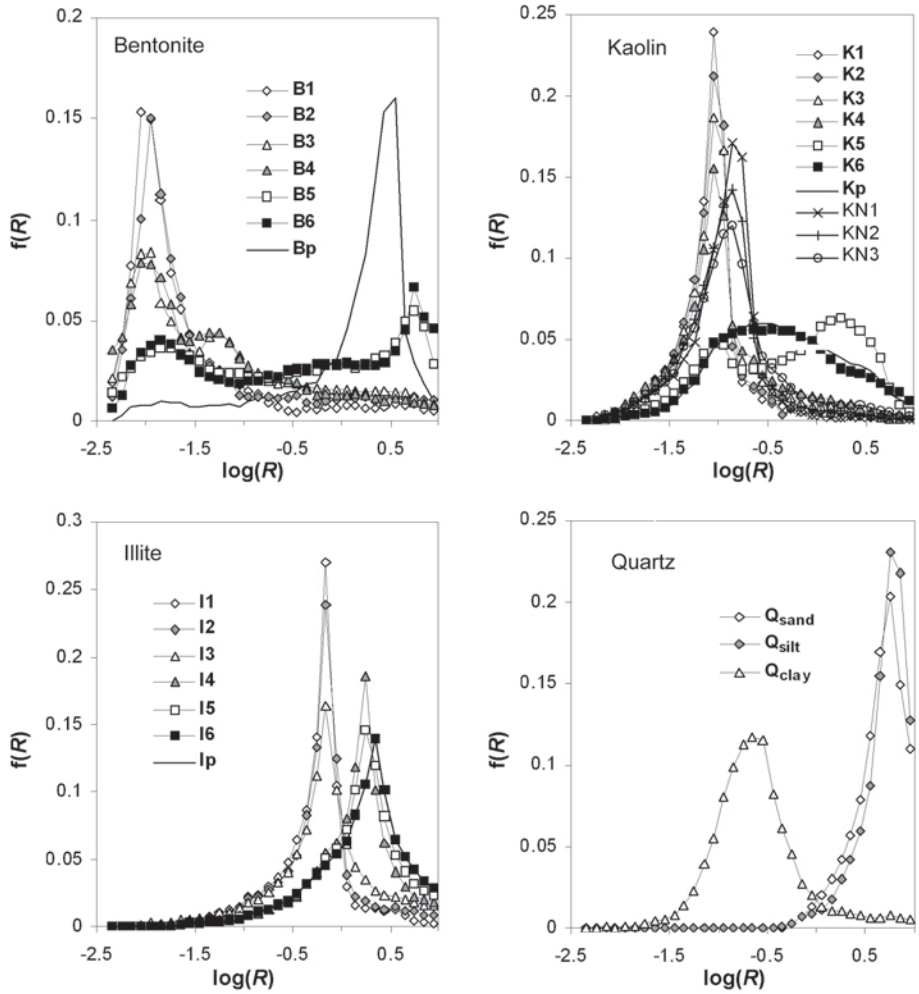

Figure 9. Mesopore-size distribution functions calculated from MIP for the minerals studied and quartz. Abbreviations of the samples as in the 'Materials' section. The number written next to the mineral abbreviation denotes size of the aggregate: 1: 4−2 mm; 2: 2−1 mm; 3: 1−0.5 mm; 4: 0.5−0.25 mm; 5: 0.25−0.09 mm; 6: <0.09. The letter p indicates powder. I = illite, K = kaolinite, KN-natural deposit of K, B = bentonite, and Q = quartz.

Apparently no coincidence exists between pore-size distributions for powders and their particle-size distributions (as presented in Figure 10). Skewing of particle-size distributions in the direction of small-particle diameters indicates the existence of particle conglomerates in the powders for quartz clay having only particles of <2 μm (preparation by sedimentation). Sedimentation of mineral suspensions also showed a negligible number of particles >2 μm (<3% w/w in all cases). The powders of bentonite and kaolinite have almost identical particle-size distributions, whereas their pore-size distributions are quite different. The similarity of the pore-size distributions for bentonite and illite is not reflected in their particle-size distributions. Neither average nor median values of powder particle diameters (median values: bentonite: 6.35; illite: 12.21; kaolinite: 10.98; and Q_{clay}: 1.85 μm) relate to the location of the pore-size distribution.

Average mesopore radii calculated from PSD curves (Figure 11) decreased with increasing mineral aggregate size, due to increase in the fraction of intra-aggregate pores within the total porosity of the sample bed (the intra-aggregate pores are apparently smaller than the pores between individual mineral grains, *i.e.* for powders of the minerals) which may also be related to changes in aggregate shape. The lack of internal porosity in quartz causes the opposite phenomenon. One concluded, then, that the smaller the quartz particles, the smaller the radius of the pores between them. That the sand-size quartz particles appear to have somewhat smaller pore radius than the silt-size particles is a direct consequence of the size of the experimental window in MIP, distinguishing pores of <10 μm. If the grains are larger than this delimiting pore dimension, larger grains have smaller average pore radii than the smaller grains due to their smaller pore-wall curvature.

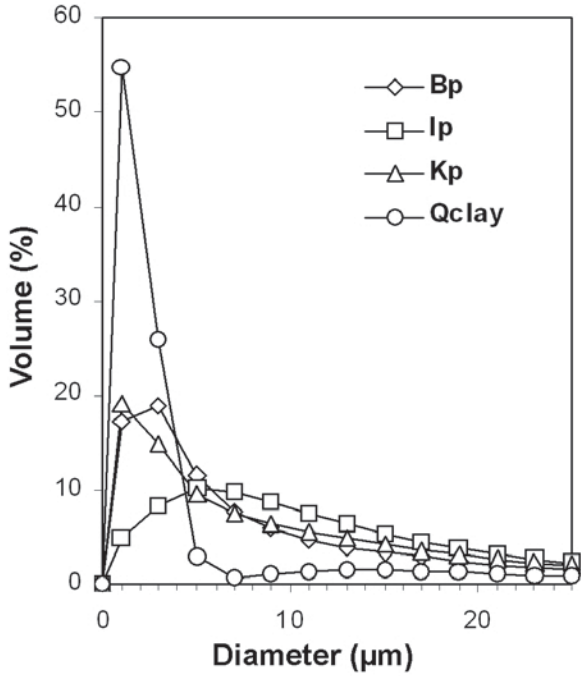

Figure 10. Particle-size distributions for powders of the minerals studied and clay-quartz. I = illite, K = kaolinite, B = bentonite, and Q = quartz.

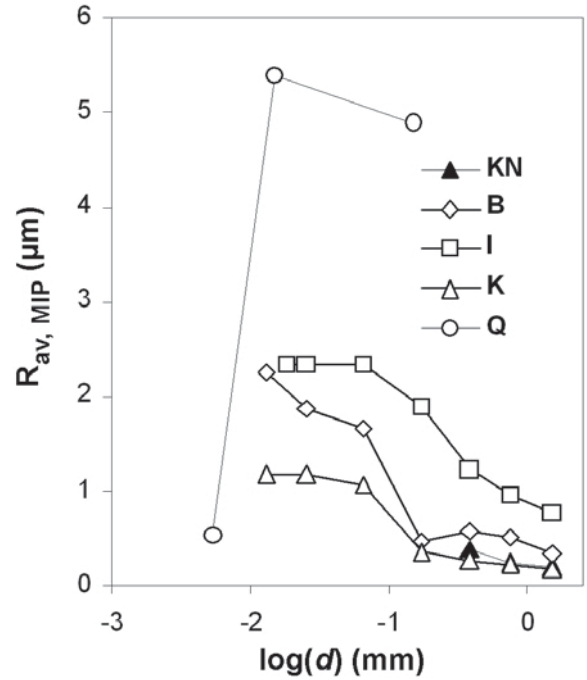

Figure 11. Mesopore (0.03−10 μm) average radii calculated from MIP for the minerals studied and quartz as related to aggregate (particle) size. I = illite, K = kaolinite, KN-natural deposit of K, B = bentonite, and Q = quartz.

The fractal plots of the materials studied are drawn based on the mercury intrusion data (Figure 12). As a rule, the fractal behavior of soil porosity occurs in a limited range of pore dimensions, referred to as upper and lower cutoffs (Pachepsky *et al.*, 1995). Fractal dimensions must be used with great care with respect to particular features of the pore structure (Crawford and Matsui 1996), so the values should be treated more as comparative parameters. The geometrical irregularities and roughness of pore surface have an essential influence on the value of the fractal dimensions, which, for porous solids, may vary from 2 to 3. The lower limiting value of 2 corresponds to a perfectly regular pore surface, whereas the upper limiting value of 3 relates to the maximum allowed pore-surface complexity. As indicated by Bartoli *et al.* (1999), the mercury porosimetry data are difficult to interpret in terms of fractal geometry because of pore connectivity effects. Those authors recommended that only the data for a very narrow range of pressures exceeding the percolation threshold should be used for computing a fractal dimension of intra-aggregate pores. Such an approach was only possible for illite and quartz. Very small fractal dimension values (close to 2) for the intra-aggregate pore system of illite and for quartz beds (see Table 2) indicate very smooth solid-pore interfaces. The D_M values calculated above penetration thresholds were <0.2 for bentonite and for kaolin (D_M values of <1.3) as illustrated in the illite section of Figure 12 (to allow better comparison between minerals) for intra-aggregate pores of the largest aggregates of these two minerals. However, the linearity of log-log plots of *dV*/*dR vs*. *R* for bentonite and kaolinite samples was found within a broad range of large pores located below the penetration threshold, and from this pore range the D_M values were calculated.

Values of fractal dimensions of the kaolinite and bentonite in relation to particle/aggregate size (Figure 13) revealed that only powders and the smallest aggregates of kaolinite (the latter seem to have been mechanically disaggregated to powders during sieving) have pore-surface fractal dimension values of <3; their large values (~2.7) indicate very complicated pore build-up. For bentonite and kaolinite aggregates, the slopes of the linear log-log plots are very large, so the calculated fractal dimensions of the pore surfaces are >3. This effect may be attributed to the suggestion that the pore structure is formed from larger voids connected by narrower necks (as for spaces between grains). Macropores are usually not interconnected with themselves (White *et al.*, 1986). Therefore, a larger void volume is attributed to a narrower neck radius for which the fractal dimension of D_M = 3 can be calculated for a cylindrical pore model. Thus, *dV*/*dR* is also greater and leads to larger D_M values. That this 'fractal dimension' increases with increasing aggregate size may be related to decreasing volumes between individual aggregates within the material bed. Gomendy *et al.* (1999) and Bartoli *et al.* (1999) showed that clay content in soil has

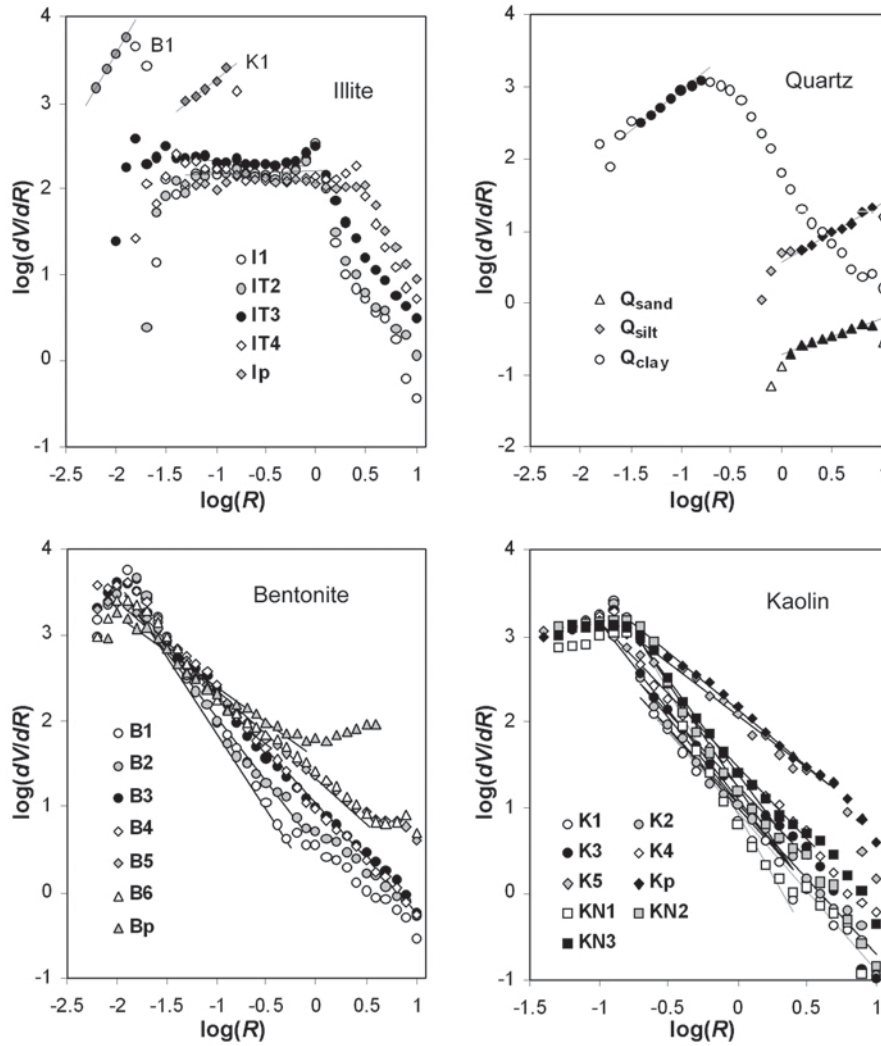

Figure 12. Fractal plots (equation 8) for the materials studied. The number written next to the mineral abbreviation denotes the size of the aggregate: 1: 4−2 mm; 2: 2−1 mm; 3: 1−0.5 mm; 4: 0.5−0.25 mm; 5: 0.25−0.09 mm; 6: <0.09. The letter p indicates powder. R = hydraulic radius. I = illite, K = kaolinite, KN-natural deposit of K, B = bentonite, and Q = quartz.

a positive effect on pore-surface fractal dimension values from mercury porosimetry data. The physical process underlying this behavior was proposed to be partial volume-pore filling by clays and, concomitantly, an increase in the rugosity of the microscopic solid:pore interfaces. As the present studies indicate, a similar effect should be observed if separate mineral aggregates are present in soil.

The comparison between the surface fractal dimensions derived from water-vapor desorption and those derived from MIP for artificially prepared aggregates of bentonite and kaolinite are shown in Figure 14. After excluding the data for kaolinite powders (black dots, Figure 14), a good negative correlation exists between both fractal dimension values. The mesopore complexity, therefore, increases with decreasing nanopore surface roughness. A less complex nanoporous structure leaves mesopore entrances which are less rugose and 'more open' so more mercury can be forced into the mesopore voids having smoother surfaces (which have larger apparent volume than voids with rough surfaces) leading to increase in D_M values.

In general, for MIP measurements of mineral pore systems, using aggregates of >1 mm is preferred. Ilavsky *et al.* (1997) concluded that MIP measurement of plasma-sprayed ceramic (alumina-titania) deposits resulted in an increase in measured porosity if the sample was fragmented into pieces of <1.2 mm effective diameter and that variation in sample thickness between 0.8 and 4.7 mm did not change the measured porosity. Laskar *et al.* (1997) stated that in studies of concrete materials, the use of mortar adhered with aggregate is preferred, rather than mortar devoid of aggregate from the same *in situ* parent concrete.

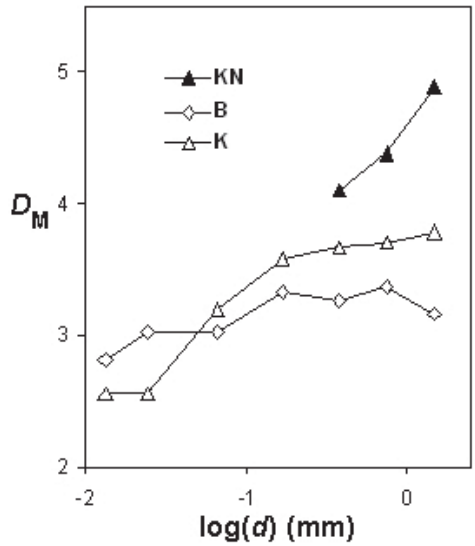

Figure 13. Mesopore fractal dimensions calculated from MIP for the minerals studied and quartz as related to aggregate (particle) size. K = kaolinite, KN-natural deposit of K, and B = bentonite.

CONCLUSIONS

Even though water vapor adsorption-desorption measurements seem to produce no artifacts due to pore connectivity, the surface properties and derived surface and nanopore parameters differ for mineral aggregates of various dimensions. With increasing aggregate size, nanopore volume and average radius increase, whereas the surface area and nanopore fractal dimensions decrease. The above changes are up to 20% of the values for powder forms of the minerals. Increases in nanopore volumes and radii are probably related to the fact that the porous structure of larger aggregates is better developed. Decreases in surface area may reflect closing of the smallest pore entrances or limited water-vapor diffusion into the aggregate body. Decreases in fractal dimensions may indicate that due to the closer location of mineral particles, water molecules cover the surface irregularities more effectively.

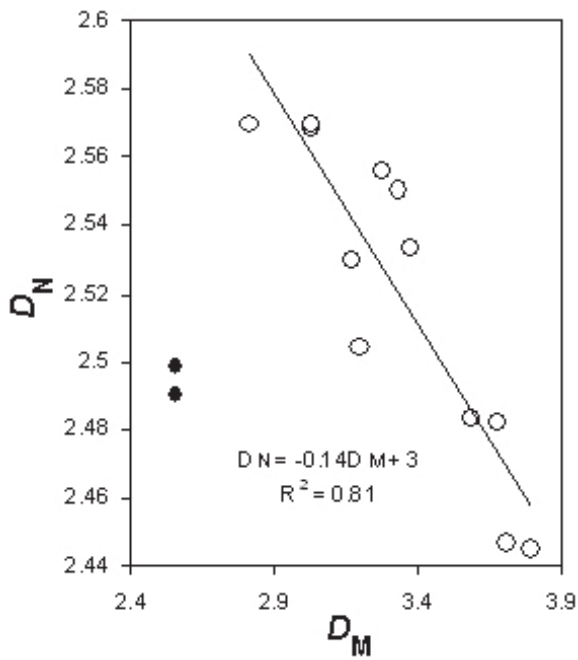

Figure 14. Relation between mesopore and nanopore surface fractal dimensions. The fitting line is drawn excluding data points marked with black dots.

Unlike the desorption technique, the mercury intrusion porosimetry readings depend heavily on the sizes of the aggregates in the sample bed to be measured. Mercury intrusion registers porosity values which are up to three times greater for samples formed from small aggregates because it is also detecting inter-aggregate pores. Extremely large porosities were measured for mineral powders. The initial part of the mercury injection curve of large aggregates was associated with 'surface defects' (the pores located at the aggregate surfaces), and the next part of the curve (rapid increase in intruded mercury) was associated with penetration of intra-aggregate pores. The penetration threshold was similar for particular mineral aggregates of different sizes and the pore throat radius at the penetration threshold decreased in the order: illite>kaolinite>bentonite. The collections of the smallest clayey aggregates were characterized mainly by inter-aggregate porosity. The mercury porosimetry data were difficult to interpret in terms of fractal geometry because calculated fractal dimensions for mineral aggregates were >3, the normal theoretical restriction. Clearly the mercury intrusion technique to estimate mineral textures requires a careful, methodical approach and interpretation of data generated. Phenomena similar to those for minerals occur for soils, though using MIP for studying soil texture may be much more complex due to the fact that soil aggregates of smaller sizes may have different particle-size compositions than larger aggregates. In both cases, testing of large aggregates is preferred.

REFERENCES

Abell, A.B., Willis, K.L., and Lange, D.A. (1999) Mercury intrusion porosimetry and image analysis of cement-based materials. *Journal of Colloid and Interface Science*, **211**, 39–44.

Alie, C., Pirard, R., and Pirard, J.P. (2001) Mercury porosimetry applied to porous silica materials: successive buckling and intrusion mechanisms. *Colloids and Surfaces, A: Physicochemical and Engineering Aspects*, **187–188**, 375–383.

Avnir, D., Farin, D., and Pfeifer, P. (1985) Surface geometric irregularity of particulate materials. The fractal approach. *Journal of Colloid and Interface Science*, **103**, 112–123.

Balci, S. (1999) Effect of heating and acid pre-treatment on pore size distribution of sepiolite. *Clay Minerals*, **34**, 647–653.

Barral, M.T., Arias, M., and Guerif, J. (1998) Effects of iron and organic matter on the porosity and structural stability of

soil aggregates. *Soil and Tillage Research*, **46**, 261–272.
Bartoli, F., Bird, N.R.A., Gomendy, V., Vivier, H., and Niquet, S. (1999) The relation between silty soil structures and their mercury porosimetry curve counterparts: fractals and percolation. *European Journal of Soil Science*, **50**, 9–22.
Baumann, D. and Keller, W.D. (1975) Bulk densities of selected dried natural and fired kaolin clays. *Clays and Clay Minerals*, **23**, 424–427.
Chung, N. and Alexander, M. (1999) Relationship between nanoporosity and other properties of soil. *Soil Science*, **164**, 726–730.
Cox, L., Celis, R., Hermosin, M.C., Becker, A., and Cornejo, J. (1997) Porosity and herbicide leaching in soils amended with olive-mill wastewater. *Agriculture, Ecosystems and Environment*, **65**, 151–161.
Crawford, J.W. and Matsui, N., (1996) Heterogeneity of the pore and solid volume of soil: distinguishing a fractal space from its non-fractal complement. *Geoderma*, **73**, 183–195.
Dullien, F.A.L. and Dhawan, G.K. (1975) Bivariate pore size distributions of some sandstones. *Journal of Colloid and Interface Science*, **52**, 129–135.
Elsharief, A.M. and Lovell, C.W. (1996) A probabilistic retention criterion for nonwoven geotextiles. *Geotextiles and Geomembranes*, 14, 601–617.
Fies, J.C. (1992) Analysis of textural porosity relative to skeleton particle size, using mercury porosimetry. *Soil Science Society of America Journal*, **56**, 1062–1067.
Gluba, T., Obraniak, A., and Gawot-Mlynarczyk, E. (2004) The effect of granulation conditions on bulk density of a product. *Physicochemical Problems of Mineral Processing*, **38**, 177–186.
Gnanapragasam, N., Lewis, B.A.G., and Fino R. (1995) Microstructural changes in sand-bentonite soils when exposed to aniline. *Journal of Geotechnical Engineering – ASCE*, **121**, 119–125.
Gomendy, V., Bartoli, F., Burtin, G., Doirisse, M., Philippy, R., Niquet, S., and Vivier, H. (1999) Silty topsoil structure and its dynamics: the fractal approach. *Geoderma*, **88**, 165–189.
Gorres, J.H., Savin, M.C., and Amador, J.A. (2001) Soil micropore structure and carbon mineralization in burrows and casts of an anecic earthworm (Lumbricus terrestris). *Soil Biology and Biochemistry*, **33**, 1881–1887.
Groena, J.C., Peffer, L.A.A., and Pérez-Ramírez, J. (2002) Incorporation of appropriate contact angles in textural characterization by mercury porosimetry. *Studies in Surface Science and Catalysis*, **144**, 91–98.
Hajnos, M. (1998) Influence of humic acid on the structural properties of kaolin – mercury porosimetry studies. *International Agrophysics*, **12**, 185–192.
Hajnos, M., Sokolowska, Z., Jozefaciuk, G., Hoffmann, C., and Renger, M. (1999) Effect of leaching DOC on pore characteristics of a sandy soil. *Journal of Plant Nutrition and Soil Science*, **162**, 19–25.
Hajnos, M., Jozefaciuk, G., Sokolowska, Z., Greiffenhagen, A., and Wessolek G. (2003) Water storage, surface, and structural properties of sandy forest humus horizons *Journal of Plant Nutrition and Soil Science*, **166**, 625–634.
Heim, A., Obraniak, A., and Gluba, T. (2005) Changes of feed bulk density during drum granulation of bentonite. *Physicochemical Problems of Mineral Processing*, **30**, 219–228.
Hollewand, M.P. and Gladden, L.F. (1992) Modelling of diffusion and reaction in porous catalysts using a random three-dimensional network model. *Chemical Engineering Science*, **47**, 1761–1770.
Ilavsky, J., Berndt, C.C., and Karthikeyan, J. (1997) Mercury intrusion porosimetry of plasma-sprayed ceramic. *Journal of Material Science*, **32**, 3925–3932.
Jaroniec, M., Kruk, M., and Olivier, J. (1997) Fractal analysis of composite adsorption isotherms obtained by using density functional theory data for argon in slitlike pores. *Langmuir*, **13**, 1280–1285.
Jarzebski, A.B., Lorenc, J., and Pajak, L. (1997) Surface fractal characteristics of silica aerogels. *Langmuir*, **13**, 1031–1035.
Jozefaciuk, G. (2001a) Comparison of soil pore characteristics obtained from desorption isotherms and mercury intrusion (in Polish). *Acta Agrophysica*, **53**, 93–100.
Jozefaciuk, G., Muranyi, A., Szatanik-Kloc, A., Farkas, C., and Gyuricza, C. (2001b) Changes of surface fine pore and variable charge properties of a brown forest soil under various tillage practices. *Soil and Tillage Research*, **59**, 127–135.
Jozefaciuk, G., Muranyi, A., and Fenyvesi, E. (2001c) Effect of cyclodextrins on surface and pore properties of soil clay minerals. *Environmental Science & Technology*, **35**, 4947–4952.
Jozefaciuk, G., Hoffmann, C., and Marschner B. (2002) Effect of extreme acid and alkali treatment on pore properties of soil samples. *Journal of Plant Nutrition and Soil Science*, **165**, 59–66.
Jozefaciuk, G., Muranyi, A., and Fenyvesi, E. (2003) Effect of randomly methylated beta-cyclodextrin on physical properties of soils. *Environmental Science & Technology*, **37**,
Kozak, E., Stawinski, J., and Wierzcho, J. (1991) Reliability of mercury intrusion porosimetry results for solids. *Soil Science*, **152**, 1325–1328.
Laskar, M.A.I., Kumar, R., and Bhattacharjee, B. (1997) Some aspects of evaluation of concrete through mercury intrusion porosimetry. *Cement and Concrete Research*, **27**, 93–105.
Lawrence, G.P. (1977) Measurement of pore sizes in fine-textured soils – a review of existing techniques. *Journal of Soil Science*, **28**, 527–540.
Mandelbrot, B. (1982) *The Fractal Geometry of Nature*. Freeman, San Francisco, USA.
Moore, C.A. and Donaldson, C.F. (1995) Quantifying soil microstructure using fractals. *Geotechnique*, 45, 105–116.
Neimark, A.V. (1996) Characterization of rough surfaces. Pp. 659–666 in: *Fundamentals of Adsorption* (M.D.D. Le Van, editor). Kluwer Academic Publishers, Boston, Massachusetts, USA.
Notario, J.S., Garcia, J.E., Caceres, J.M., Arteaga, I.J., and Gonzalez, M.M. (1995) Characterization of natural phillipsite modified with orthophosphoric acid. *Applied Clay Science*, **10**, 209–217.
Pachepsky, Y.A., Polubesova, T.A., Hajnos, M., Sokolowska, Z., and Jozefaciuk, G. (1995) Fractal parameters of pore surface area as influences by simulated soil degradation. *Soil Science Society of America Journal*, **59**, 68–75.
Pagliali, M., Raglione, M., Panini, T., Maletta, M., and La Marca M. (1995) The structure of two alluvial soils in Italy after 10 years of conventional and minimum tillage. *Soil and Tillage Research*, **34**, 209–223.
Penumadu, D. and Dean, J. (2000) Compressibility effect in evaluating the pore-size distribution of kaolin clay using mercury intrusion porosimetry. *Canadian Geotechnical Journal*, **37**, 393–405.
Perez, P., Todoroff, P., Touma, J., and Fortier M. (1999) Determining the hydraulic properties of a Sahelian crusted soil. 1. In field experiment and measurements. *Agronomie*, **19**, 331–340.
Perrier, E., Bird, N., and Rieu, M. (1999) Generalizing the fractal model of soil structure: the pore-solid fractal approach. *Geoderma*, **88**, 137–164.
Ringrose-Voase, A.J. and Bullock, P. (1984) The automatic recognition and measurement of soil pore types by image analysis and computer programs. *Journal of Soil Science*, **35**, 673–684.

Romero, E., Gens, A., and Lloret, A. (1999) Water permeability, water retention and microstructure of unsaturated compacted Boom clay. *Engineering Geology*, **54**, 117–127.

Rouquerol, R., Avnir, D., Fairbridge, C.W., Everett, D.H., Haynes, J.H., Pernicone, N., Ramsay, J.D.F., Sing, K.S.W., and Unger, K.K. (1994) Recommendations for the characterization of porous solids. *Pure and Applied Chemistry*, **66**, 1739–1758.

Rouquerol, F., Rouquerol, J., and Sing, K. (1999) *Adsorption by Powders and Porous Solids*. Academic Press, London.

Schaffer, C.E., Arands, R.R., van der Sloot, H.A., and Kosson, D.S. (1997) Modelling of the gaseous diffusion coefficient through unsaturated soil systems. *Journal of Contaminant Hydrology*, 29, 1–21.

Sing, K.S.W. (1982) Reporting physisorption data for gas/solid systems with the special reference to the determination of surface area and porosity. *Pure and Applied Chemistry*, **54**, 2201–2218.

Sokolowska, Z. and Sokolowski, S. (1999) Influence of humic acid on surface fractal dimension of kaolin: analysis of mercury porosimetry and water vapour adsorption data. *Geoderma*, **88**, 233–249.

Sposito, G. (1984) The solvent properties of adsorbed water. Pp. 69–72 in: *The Surface Chemistry of Soils* (G. Sposito, editor). Oxford University Press, New York.

Srasra, E. and Trabelsi-Ayedi, M. (2000) Textural properties of acid activated glauconite. *Applied Clay Science*, **17**, 71–84.

Suarez Barrios, M., Flores González, L.V., Vicente Rodríguez, M.A., and Martín Pozas, J.M. (1995) Acid activation of a palygorskite with HCl: Development of physico-chemical, textural and surface properties. *Applied Clay Science*, **10**, 247–258.

Temuujin, J., Jadamba, T., Burma, G., Erdenechimeg, S., Amarsana, J., and MacKenzie, K.J.D. (2004) Characterisation of acid activated montmorillonite clay from Tuulant (Mongolia). *Ceramics International*, **30**, 251–255.

Thompson, A.H., Katz, A.J., and Krohn, C.E. (1987) The microgeometry and transport properties of sedimentary rocks. *Advances in Physics*, **36**, 625–694.

Van Damme, H. (1998) Structural hierarchy and molecular accessibility in clayey aggregates. Pp. 55–74 in: *Fractals in Soil Science* (P. Baveye, J.Y. Parlange, and B.A. Stewart, editors). CRC Press, Boca Raton, Florida, USA.

Van Damme, H., Levitz, P., Bergaya, F., Altcover, J.F., Gatineau, L., and Fripiat, J. (1986) Monolayer adsorption on fractal surfaces: a simple two-dimensional simulation. *Journal of Chemical Physics*, **85**, 616–624.

Volzone, C. and Hipedinger, N. (1997) Mercury porosimetry of compacted clay minerals. *Zhurnal of Pflanzenernaehrung und Bodenkunde*, **160**, 357–360.

White, R.E., Dyson, J.S., Gerstl, Z., and Yaron B. (1986) Leaching of herbicides through undisturbed cores of a structured clay soil. *Soil Science Society of America Journal*, **50**, 277–283.

Yokoya, N., Yamamato, K., and Funakuro, N. (1989) Fractal-based analysis and interpolation of 3D natural surface shapes and their application to terrain modelling. *Computer Vision Graphics and Image Processing*, **46**, 284–302.

(*Received 27 February 2008; revised 3 April 2009; Ms. 0130; A.E. P. Malla*)